Journal of Pharmaceutical Innovation (2023) 18:756–767
https://doi.org/10.1007/s12247-023-09725-6

ORIGINAL ARTICLE

Synthesis and Anticancerogenic Effect of New Generation Ruthenium-Based Nanoparticle from *Homalothecium sericeum* with Eco-Friendly Method

Nourhan Samir[1] · Dilşad Özerkan[2] · Ferdane Danışman-Kalındemirtaş[3] · İshak Afşin Kariper[4] · Huri Bulut[5] · Dürdane Serap Kuruca[6] · Ergin Murat Altuner[7] · Engin Ulukaya[5]

Accepted: 14 March 2023 / Published online: 31 May 2023

Abstract

Background Green synthesis is a simple, inexpensive, and highly efficient method for the preparation of nanoparticles. In this study, ethanol extracts of *Homalothecium sericeum* (HOM) moss were used as reducing agents for the synthesis of biocompatible ruthenium nanoparticles (RuNPs). The ruthenium-based green synthesis method has not been used in any other work in the literature. UV–visible spectrophotometer (UV–Vis), Zetasizer, FTIR, and EDX-SEM were used to characterize the RuNPs synthesized by the green synthesis method, and their efficacy on cell viability was tested on HCT116 human colon cancer cells.

Methods UV spectroscopic measurements were used to study the release of HOM-RuNPs. Apoptosis was assessed by measuring protein expression of p53, Bax, and Bcl-2 by Western blotting. The presence of apoptosis was confirmed by double staining with Hoechst dye/propidium iodide under a fluorescence microscope. HOM-RuNPs were also tested for BCRP/ABCG2 expression to check for drug resistance.

Results HOM-RuNPs with a size of 70–80 nm were found to be most effective at a dosage of 5.71 µg/ml and induced cell death by increasing the ratio of Bax/Bcl-2 and p53 expression. It was also shown to reduce multidrug resistance protein (ABCG2), suggesting that it may be useful against multidrug resistance.

Conclusion Ruthenium-based nanoparticles synthesized by a green synthesis technique may be a candidate for anticancer drugs in the pharmaceutical industry and deserve further attention for proof-of-concept studies.

Keywords Ruthenium nanoparticles · Green synthesis · Apoptosis · *Homalothecium sericeum*

✉ Dilşad Özerkan
dilsadokan@gmail.com

1 Molecular Cancer Research Center, Istinye University, Istanbul, Turkey

2 Department of Genetic and Bioengineering, Faculty of Engineering and Architecture, Kastamonu University, Kastamonu, Turkey

3 Department of Physiology, Faculty of Medicine, Erzincan Binali Yıldırım University, Erzincan, Turkey

4 Department of Science Education, Education Faculty, Erciyes University, Kayseri, Turkey

5 Department of Medical Biochemistry, Faculty of Medicine, Istinye University, Istanbul, Turkey

6 Department of Physiology, Medical Faculty, Basic Medical Sciences, Istanbul Atlas University, Istanbul, Turkey

7 Department of Biology, Faculty of Science, Kastamonu University, Kastamonu, Turkey

Introduction

The fourth leading cause of death in the world and the third most common cancer is colorectal carcinoma (CRC), a malignant tumor of the epithelium of the colon or rectum [1]. According to statistics, colorectal cancer is the second and third most common cancer in both men and women, respectively [2]. Surgical resection, radiation, and chemotherapy are the mainstays of conventional colorectal cancer treatment, and they can increase the survival rate from 90% of stage I patients to 10% of stage IV patients by only 5 years [3]. Although surgery is a necessary component of CRC treatment, it can lead to postoperative problems such as tumor cell recurrence and/or liver metastases. Peripheral neuropathy and bowel dysfunction are long-term side effects of chemotherapy and radiotherapy that are becoming more common and urgent [4]. Most of the genetic instability in

CRC is caused by chromosomal instability, which is defined by a significant gain or loss of all or most chromosomes [5].

The rare noble metal ruthenium can form complexes with a variety of ligands, but is not present in biological systems [6]. Due to the special properties of ruthenium, potential antitumor and antimetastatic therapies have been developed. Although platinum-based (Pt) anticancer drugs are commonly used in cancer therapy, their toxicity and the resistance of colorectal cancer cells to Pt treatments have sparked interest in the search for alternative metal-based therapies. Due to its central location in the second row of the transition metal series, Ru exhibits both early and late transition metal characteristics. Ru has a partial full 4d subshell with many values that allow it to generate a wide range of compounds through bond formation that can act as antitumor agents against various cancer cell types [7]. Several additional elements with different chemical "hardness" and electronegativity can also form robust chemical bonds with ruthenium. This property enables binding to a whole range of biomolecules [8]. Observations suggest that Ru complexes control many cellular signaling pathways either directly or indirectly related to cell growth, reproduction, proliferation, and migration signaling to exert their antitumor effects in colorectal carcinoma [9]. In addition, it was discovered that Ru complexes can cause apoptosis by generating too many reactive oxygen species (ROS) and damaging cellular organelles that are necessary for cell viability [10]. Five different Ru complexes (II) were synthesized and shown to be more potent antiproliferative than cisplatin in an in vivo study using a CT26 colon carcinoma mouse xenograft model. In fact, one of them was found to have a cytotoxic effect that limited tumor growth [11].

The use of hazardous solvents is the major limitation of nanoparticles [12]. Besides toxicity, these chemical reagents also have negative effects on the ecosystem [13]. Moreover, increasing the temperature in the environment of the starting material requires a lot of space, generates a lot of heat, and requires a significant amount of time in the physical synthesis of nanoparticles. Therefore, green synthesis represents a reliable, biocompatible, and environmentally friendly technique for the production of NPs for a wide range of applications, e.g., in the biomedical field [14]. Green synthesis is carried out by fungi, algae, bacteria, and plants [15, 16] and is more efficient, simpler, less expensive, and can be easily implemented. In addition, large-scale cultivation is not required, and the process does not pose a biological risk as is the case with nanoparticle synthesis using microorganisms [17]. Green production of nanoparticles in the size range of 1–100 nm involves the biological reduction of metal ions to their basic constituents using plants or plant tissues [15].

To date, no research based on Ru nanoparticles using the green synthesis approach has been discovered. The first green plant that evolved through the process of natural selection and effectively adapted to its environment is bryophytes [18]. Since moss can develop in any environment, it is very easy to acquire. *Homalothecium sericeum* is widely distributed in Turkey. In our previous study, ethanol extract of *H. sericeum* (HOM), the moss plant to be used in the study, showed the greatest antiproliferative activity at low concentration, so it was selected for this study [19]. In another study, this species belonging to the Brachytheciaceae family was found to have antibacterial and antiproliferative activity [20]. Due to the negative effects of chemotherapy drugs, alternative treatments are currently being explored. Moreover, we thought that the efficacy of *H. sericeum* would be improved if it was delivered to the desired site with the new nanocarrier. Therefore, this time, the researchers wanted to investigate the effect of Ru nanocarrier produced by green synthesis using the plant HOM on the survival and apoptosis of HCT116 colon cancer cells.

Material and Methods

Extraction of *Homalothecium sericeum*

The extracts of *Homalothecium sericeum* were obtained by lyophilization. The dried herbarium specimens of the algae used for extraction were properly cleaned with sterile distilled water before being allowed to dry in the shade. The dry samples were ground in porcelain mortars and pestles. The dry moss samples were ground into powder in the mortar after the hands of the mortar and pestle were properly washed with 70% ethyl alcohol. After 3 days of continuous mixing at 120 to 160 rpm at room temperature, the samples were prepared into powder form.

The solvent used was absolute ethyl alcohol, which has a boiling point of 78.37 °C and a relative polarity of 0.654. The ratio of sample to solvent during extraction was set at 1:50. The extracts were filtered at the end using Whatman paper No. 1 (Merck Cat. No.: WHA1443090). After a 24-h extraction period, the solutions were thoroughly evaporated at 40 °C under vacuum in a rotary evaporator (Heidolph) and stored at − 80 °C until all water phases were completely dried. Dimethyl sulfoxide (DMSO) (Sigma Cat. No. D8418) was used to dilute the dry, powdered extracts before they were used for analysis [21].

Preparation of HOM-RuNPs

Fifty milliliters of water was used to dissolve 0.1 mM $RuCl_3$ and prepare a stock solution. After sonication in an ultrasonic bath for 1 h with 1 ml each of the stock solution of black algal plant extract at a concentration of 11.42 mg/ml and the Ru stock solution, ruthenium-based nanoparticles were prepared by the green synthesis technique.

Characterization of HOM-RuNPs

Zeta Sizer Measurements

Zetasizer measurements were performed at room temperature. Dynamic light scattering (DLS) measurements were performed on RuNPs samples using the Zetasizer Nano ZS with a 4 mW He-Ne laser at a wavelength of 633 nm and a detection angle of 173°.

FTIR Analyses

Fourier transform infrared spectroscopy (FTIR) experiments were performed with the instrument BRUKER ALPHA in diffuse reflectance mode with a resolution of 4 cm × 1. To obtain a satisfactory signal-to-noise ratio, 10 scans were acquired.

EDX-SEM Analyses

RuNPs and HOM-RuNPs were dropped onto a glass substrate and coated with 45 A^0 Au/Pd using a Polaron sc 7620 small spray coater for SEM and EDX studies. Imaging was performed for liquid samples by pouring them onto glass surfaces and connecting them to the instrument after drying.

Absorption Measurements

The Hach Lange DR 5000 spectrophotometer was used to evaluate the absorbance of aqueous solutions of plastics. Water was used as a standard for the reference part of the spectrophotometer and the solutions prepared for the sample part were used as a reference for measurements in the wavelength range 200–1100 nm.

Release Analysis of Ruthenium-Based Nanoparticles

PBS buffer solution with a pHof 7.4 served as the medium, and a dialysis membrane was used to monitor the release of HOM loaded onto the ruthenium nanocarrier. On a 1 mg/ml nanocarrier, 2 ml of HOM-RuNPs was transported to the dialysis membrane. The ambient temperature is about 37 °C, and the dialysis membrane is about 16 cm long (Sigma Aldrich company, average flat width 10 mm, typical molecular weight cut-off = 14,000). The dialysis membrane was sealed at both ends. The release of HOM, loaded onto the nanocarrier in the dialysis membrane, was monitored for 50 h while immersed in 50 ml of buffer solution with a pH of 7.4. HOM-RuNPs were used to prepare 5 different concentrations, and the absorbance of each concentration was measured at 290 nm using the UV spectrophotometer.

Colorectal Cancer Cell Culture

The human colorectal cell line (HCT116) was used for this study, considering that our previous work with HOM ethanol extract was successful in HCT116 cells [19]. Cell density was 80% after cells were cultured in T75 culture flasks with DMEM containing 10% FBS and 1% penicillin/streptomycin. Subsequently, 5000 cells were seeded in 96 wells, and the mixture was incubated at 37 °C and 5% CO_2. In a previous study, the most effective dosage was found to be 11.42 g/ml. In this study, HOM-RuNPs were administered at doses of 11.42, 5.71, 2.85, 1.42, 0.42, and 0.35 µg/ml for a total of six administrations and incubated again for 48 h. The sulforhodamine B assay (SRB) was used to evaluate the antiproliferative activity of HOM and HOM-RuNPs against the colon cancer cell line (HCT116). In contrast to 3-(4,5-dimethylthiazol-2-yl)-2,5-diphenyltetrazolium bromide, this technique does not demonstrate metabolic activity (MTT). The primary pathway by which SRB identifies living cells is by stoichiometric binding to proteins rather than by interaction of metabolic activity with this dye [22]. Dose–response curves were generated to determine the IC_{50} (concentration that inhibits the growth of 50% of cells) of the compounds. The efficacy of the extracts was evaluated with respect to this criterion.

HOECHST 33342/Propidium Iodide (PI) Double Immunostaining

A total of 5000 cells/100 µl HCT116 cells were plated on 96-well plates. After applying HOM, RuNPs, and HOM-RuNPs IC90 (90% reduction dose of cell viability), a 24-h staining technique was performed with Hoescht33342 (ThermoFisher) and propidium iodide (PI) (BioLegend). The wells, whose supernatants were obtained from the working solution prepared at 1 g/ml and incubated at room temperature in the dark, received 50 µg/ml of each dye. A Nikon Eclipse Ts2 immunofluorescence microscope was used to acquire the images.

Western Blotting

For cell lysates, the Bradford technique was used, and 1 mg/ml bovine serum albumin (BSA) was used as a reference. Quantification of total protein was performed in a plate reader at a wavelength of 595 nm (Thermo Scientific Multiskan FC, 2011-06, USA). For each sample, 20 µg of total protein was added to SDS-PAGE. The instrument was run at 120 mV for 1 h. Following the run, protein samples were

transferred to PVDF membranes from the gel where they were incubated at 110 mV for 10 min (Biorad, USA). The membranes were occluded after transfer. The membranes were blocked by treatment in 5% skim milk for 1 h at room temperature in an orbital shaker. After blocking, membranes were washed with TBS-T five times for 5 min. Primary antibodies against β-actin (Cell signaling, 4970, USA), BCRP/ABCG2, p53 (Abcam, 32389, UK), Bax (Elabscience, E-AB-13814, USA), and Bcl2 (GeneTex, GTX100064, USA) were prepared in 2.5% skim milk at 1/1000, 1/500, 1/750, 1/200, and 1/200 ratios, respectively. The membranes were incubated in a shaker at +4 °C for one night after labeling with the primary antibodies. Membranes were labeled with 1/1000 secondary antibody (Santa Cruz Biotechnology, Inc., Santa Cruz, CA, USA) and shaken at room temperature for 1 h before washing with TBS-T. Fusion Fx5 instrument (Vilbert Laurmart) was used to examine and evaluate the antibody bands.

Statistical Analyses

Results are expressed as the mean standard deviation of experiments repeated at least three times (±SD). GraphPad Prism 5 was used to calculate the Kruskal–Wallis test and one-way analysis of variance (ANOVA) between groups. Significant results were defined as $p < 0.05$, and highly significant results as $p < 0.01$. The IC_{50} was calculated using the IC_{50} Calculator (AAT Bioquest) (https://www.aatbio.com/tools/ic50-calculator).

Results

Characterization Results

The absorption peak of ruthenium was visible in the UV-VIS spectrum at 280 nm, although somewhat weaker (Fig. 1). The UV-VIS spectrum of this algal extract showed absorption peaks when the HOM plant extract surrounded and bound to Ru molecules. A large absorption peak, originating from n-* rather than -* transitions, can be seen at 414 nm, although the absorption peak is visible from electronic -* transitions originating from both aromatic structures and double bonds, i.e., chromophore groups. Thus, there must be other electrons in the materials besides the n-electrons that cause this transition. Another name for this is hypochromic transition. These transitions are caused by the O, N, etc. structure. It is caused by the unshared electron pairs of the doubly bonded electroatoms, as well as the polar groups of the solvents - OH - forming hydrogen bonds with the unshared electron pairs of the molecule.

A look at the FTIR analysis shows the -NH peak at 3329 cm^{-1}, aliphatic—CH peaks at 2912–2852 cm^{-1}, aldehyde, amino acid, carboxylic acid, or other functional group-C = O bond vibrational peaks at 1725 cm^{-1},—OH voltage peak at 1591 cm^{-1}, and -N = O asymmetric voltage peak at 1396 cm^{-1}. The C–O–C ester vibrational peak is at 1222 cm^{-1}. O–Ru–O vibrational peaks caused by Ru metal

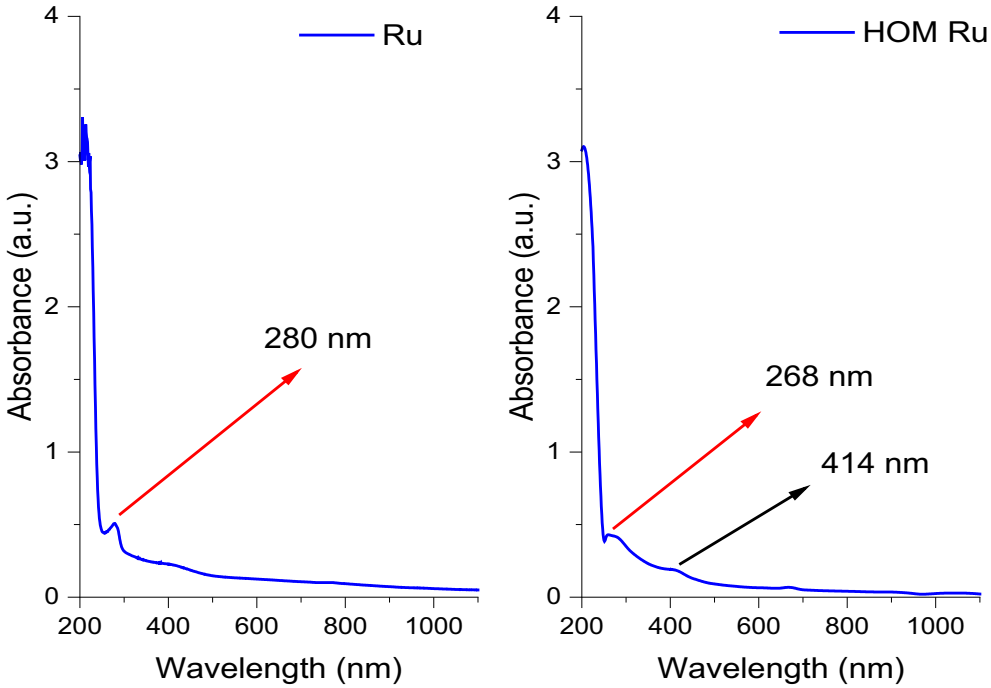

Fig. 1 UV-VIS spectrum of RuNPs and HOM-RuNPs

are seen at 840 cm^{-1}, as in the literature (Joshi et al. [23]), and vibrational signals from aromatic compounds were found at 700–450 cm^{-1} wavenumber. -C- OH, belonging to groups such as carboxylic acid aldehydes, at 1048 cm^{-1} vibrational peak, O–Ru–O vibrational peaks due to Ru metal are observed at 840 cm^{-1} (Fig. 2). UV–VIS spectra show that the structure has absorption peaks related to the electronic transitions of carboxylic acids, aldehydes, amine groups, and hydroxyl groups.

The Zetasizer Nano ZS device was used to measure the size of nanoparticles in nanoparticle solutions (Fig. 3). The result was that the diameters of Ru nanoparticles prepared by green synthesis from moss plant extract ranged from 32.67 to 164.2 nm. Most of the particles were still between 50 and 60 nm in size. The derived count rate (kcps), which is also a measure of the number of nanoparticles in the environment, was 255, and the PDI values, which are a measure of the maturity of the nanoparticles, were 0.560. The surface potential was − 53.1 mV, while the conductivity of the solution was measured as 0.172 mS/cm. It is known that cancer cells can benefit from a negative surface potential [24].

According to FESEM images, the particle size of a particle trapped on the 100 nm scale is between 70 and 80 nm (Fig. 4). This result agrees quite well with measurements made with the Zeta Sizer. In EDX analyses, the relative proportions of elements in the samples are reported (Fig. 5). Since the samples were dried overnight on a glass substrate in a sterile environment at room temperature, a very distinct Si peak can be seen. Ruthenium was bound to the C, N, and O components of the moss, and 0.14% Ru was also identified in the structure. This proves that ruthenium is present in the structural composition of moss.

Release Findings of HOM-RuNPs

To evaluate the release profile of the drug, the release of the drug from the nanocarrier loaded with HOM was performed at physiological pH, pH 7.4. According to the UV results, the wavelength of HOM moss extract was set at 480 nm. From the measurements performed at different times at this wavelength, the release of HOM from the Ru nanocarrier was cumulative, especially in the first phase. The release of the drug occurred within 10–12 h, and the percentage of release reached about 85% within 12 h (Fig. 6). According to the UV results, the cumulative HOM release rate of HOM-RuNPs seems to increase gradually over time. Moreover, the fact that HOM from RuNPs has a high release rate of 85% is important for reaching the targeted cancer cells with a high rate of extract effect.

Cell Viability Findings

HCT116 cell growth suppression at 5.71 µg/ml was shown to be the most effective dosage (Fig. 7).

HOM had an IC50 of 10.0764 µg/ml, whereas HOM-RuNPs had an IC_{50} of 5.2131 µg/ml, as shown by the IC_{50} values of HCT116 cells (Fig. 8).

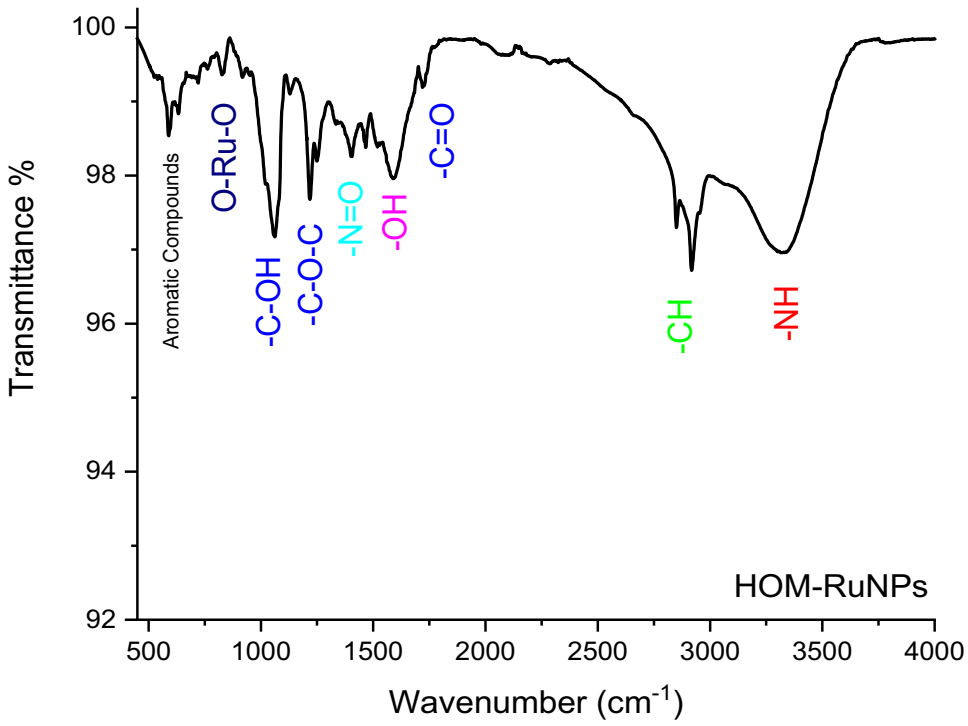

Fig. 2 FTIR analysis of HOM-RuNPs

Size d.nm	Mean Number %	Std Dev Number %
0,4000	0,0	
0,4632	0,0	
0,5365	0,0	
0,6213	0,0	
0,7195	0,0	
0,8332	0,0	
0,9649	0,0	
1,117	0,0	
1,294	0,0	
1,499	0,0	
1,736	0,0	
2,010	0,0	
2,328	0,0	
2,696	0,0	
3,122	0,0	
3,615	0,0	
4,187	0,0	
4,849	0,0	

Size d.nm	Mean Number %	Std Dev Number %
5,615	0,0	
6,503	0,0	
7,531	0,0	
8,721	0,0	
10,10	0,0	
11,70	0,0	
13,54	0,0	
15,69	0,0	
18,17	0,0	
21,04	0,0	
24,36	0,0	
28,21	0,0	
32,67	0,1	
37,84	6,4	
43,82	19,8	
50,75	26,6	
58,77	21,8	
68,06	13,4	

Size d.nm	Mean Number %	Std Dev Number %
78,82	6,8	
91,28	3,0	
105,7	1,2	
122,4	0,4	
141,8	0,2	
164,2	0,1	
190,1	0,0	
220,2	0,0	
255,0	0,0	
295,3	0,0	
342,0	0,0	
396,1	0,0	
458,7	0,0	
531,2	0,0	
615,1	0,0	
712,4	0,0	
825,0	0,0	
955,4	0,0	

Size d.nm	Mean Number %	Std Dev Number %
1106	0,0	
1281	0,0	
1484	0,0	
1718	0,0	
1990	0,0	
2305	0,0	
2669	0,0	
3091	0,0	
3580	0,0	
4145	0,0	
4801	0,0	
5560	0,0	
6439	0,0	
7456	0,0	
8635	0,0	
1,000e4	0,0	

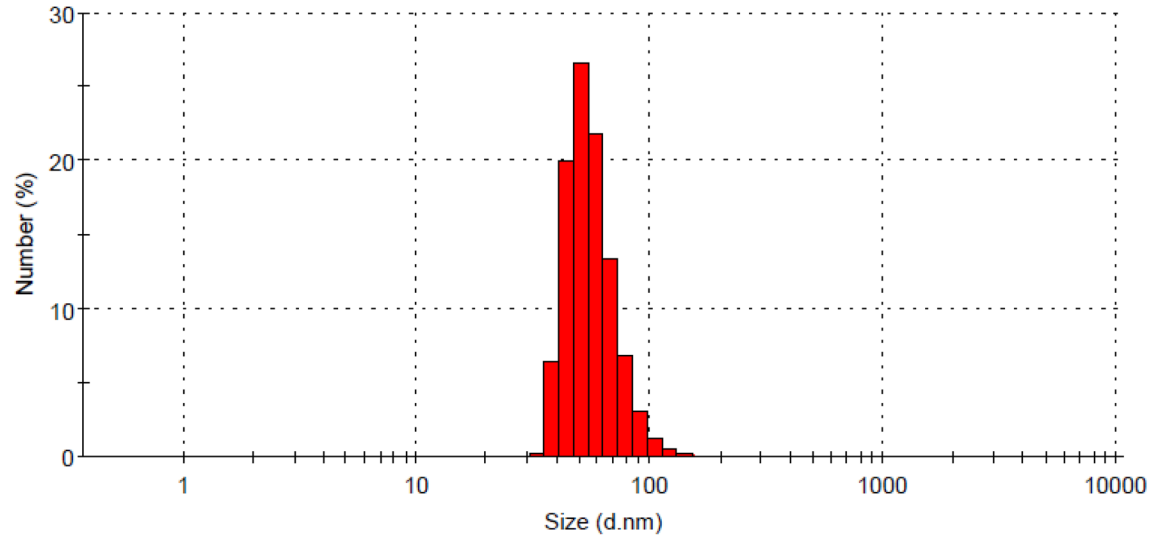

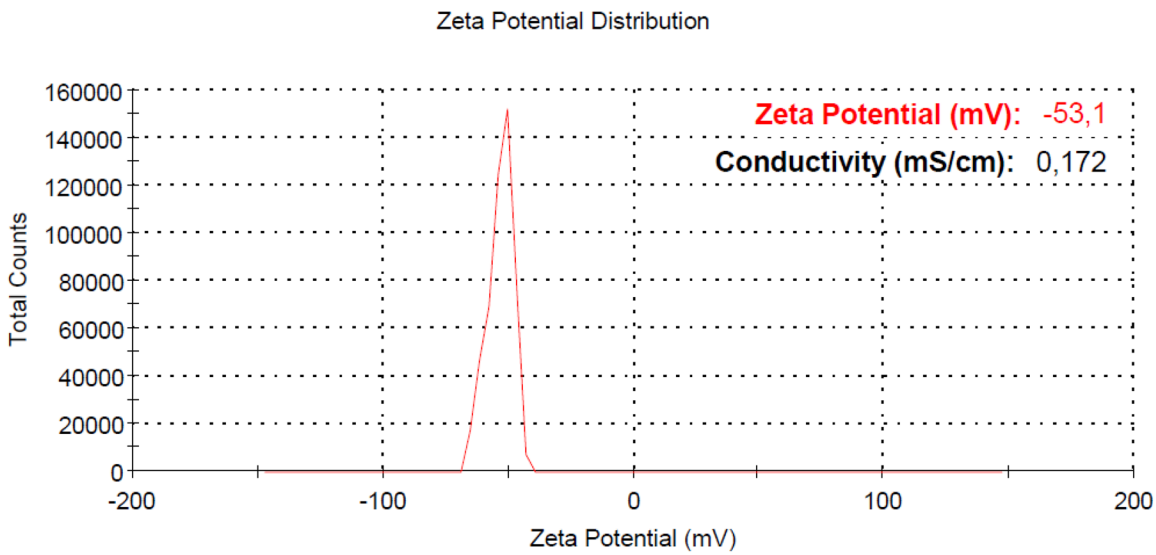

Fig. 3 Zeta potential measurement of HOM-RuNPs

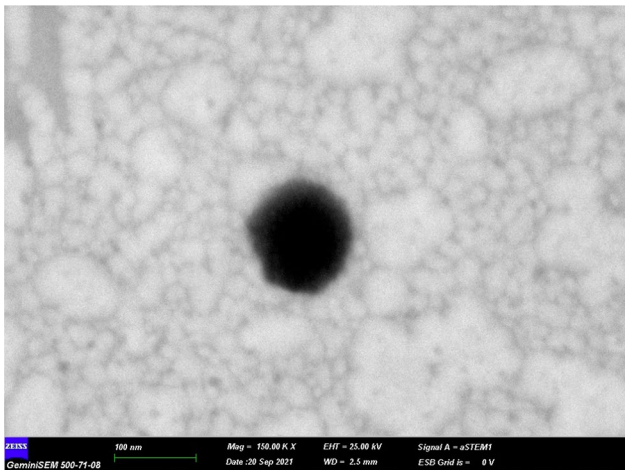

Fig. 4 FE-SEM image of HOM-RuNPs

Double Flourescent Staining for Apoptosis

Hoechst 33,342 is used for nuclear staining of both live and dead cells, whereas propidium iodide (PI) is used only to determine primary or secondary necrotic (apoptotic) cells, as it is pumped out of living cells [25]. After HOM-RuNP application, apoptosis was significantly increased compared with the control group. The percentage of dead cells was lower in the HOM-treated group than in the HOM-RuNP-treated group (Fig. 9). And although the dose of HOM-extract in the green-synthesized Ru nanocarrier was lower than the concentration in the HOM-treated group, it was clear that apoptosis increased in HCT116 cells.

Administration of HOM-RuNPs to HCT116 cells significantly increased Bax/Bcl-2 and p53 expressions and protein levels ($*p < 0.05, **p < 0.001$). Comparing the effect of HOM and HOM-RuNPs on colorectal cells, a remarkable increase in apoptotic proteins is observed (Fig. 10a, b). Therefore, in this study, apoptosis was found to occur via the intrinsic pathway. This intrinsic pathway could include mitochondria (due to the increased Bax/Bcl-2 ratio) and DNA damage (due to the increase in p53).

ABCG2 expression level was shown to be significantly reduced ($p < 0.05$). While drug resistance in the control group was quite high at the beginning of this study, it is important to note that after treatment with HOM-RuNPs, ABCG2 levels decreased significantly (Fig. 10c).

Discussion

Conventional techniques for synthesizing NP, such as physical and chemical processes, pollute the environment with their harmful byproducts. Therefore, green synthesis, one of the solutions to avoid this and using plants, has recently gained popularity. The production of nanoparticles using green synthesis is simple, inexpensive, and extremely effective. The phytochemicals of plant extracts are used as reducing agents to reduce the toxicity of NPs [26]. Due to the slower kinetics, ease of manipulation, and control over crystal formation to stabilize nanoparticles, green synthesis has been shown to be a superior approach for the sustainable, safe production of nanoparticles [27]. Since ruthenium is less harmful to normal cells, more easily absorbed by tumor cells, and rapidly eliminated from the body, it may be preferred [28]. One of its main advantages is its ability to specifically localize and bind tissues of patients, which is enabled by its ligand structure [29]. By binding to DNA crosslinks at multiple sites, it has shown therapeutic activity in cisplatin-resistant malignancies, unlike platinum [30]. Although Ru-based nanoparticles possess all these desirable properties, there are few studies on them [31–34]. In this research, the marine alga *Dictyota dichotoma*, a natural antioxidant, was used

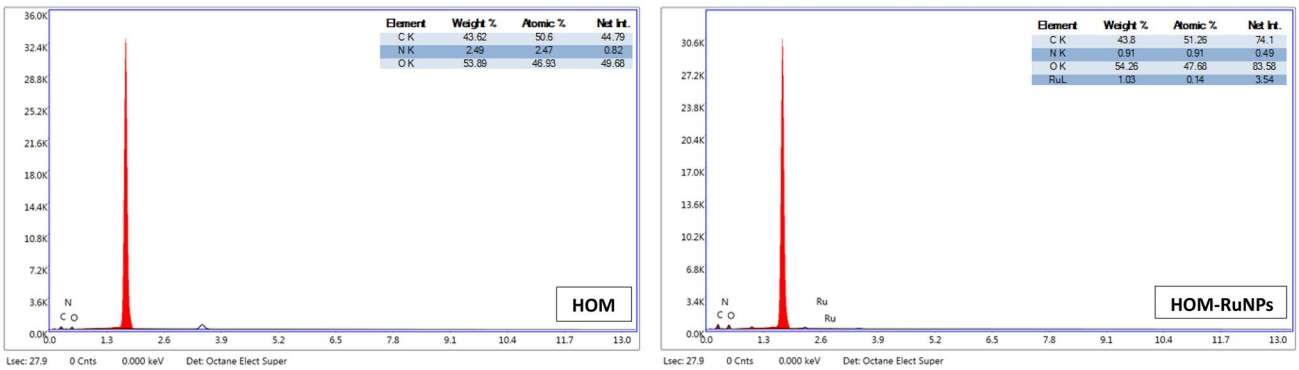

Fig. 5 EDX measurement of HOM and HOM-RuNPs

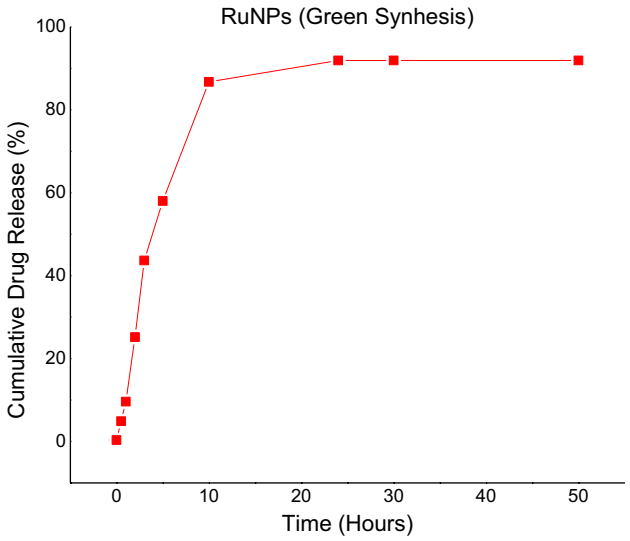

Fig. 6 It displays the cumulative proportion of HOM-RuNPs release

to synthesize ruthenium nanoparticles, which were then tested on the cancer cell lines Hela, MCF-7, and VERO. RuNPs with an average size of 30 nm were found to be harmful at low doses in all 3 cell lines [31]. Similarly, HOM-RuNPs produced with a size of 70–80 nm significantly reduced the viability of colon cancer cells at modest doses. The effect was even twice that of the group receiving only HOM plant supplements. So, the nanoparticles we developed were very successful. Other studies focus only on the antibacterial abilities of RuNPs [32, 33]. As a result, there are many things that need to be clarified.

Nanoparticles selectively accumulate in tumors due to increased permeability and insufficient lymphatic drainage.

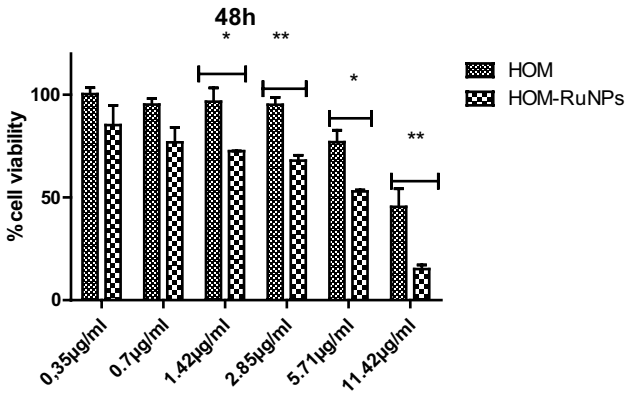

Fig. 7 The graph shows the difference in viability of all groups at each dose after 48 h. (*$p < 0.005$, **$p < 0.001$, vs. both groups)

The permeability and retention of a disrupted vascular and tumor microenvironment (TME) can lead to a 70-fold increase in macromolecule accumulation in the TME and is referred to as the enhanced permeability and retention (EPR) effect. This leads to non-uniform flow in the tumor, increased interstitial fluid pressure due to fluid extravasation, hypoxia, and an overacidified environment, among other effects. The ability of EPR-based drug carriers to overcome these obstacles depends on several aspects, including drug absorption, selectivity, and nanoparticle diameter, morphology, and interfacial properties [35]. Passive targeting is mainly based on a dispersion mechanism. Therefore, size is a crucial factor for the EPR-dependent delivery process. Shape and morphology also play an important role in passive targeting. Solid, spherical particles between 50 and 200 nm in size generally flow long enough not to be absorbed by the liver and spleen. However, their mass is sufficient to hinder excretion via the kidneys. Therefore, it is possible to control EPR-dependent drug transport by changing the diameter, morphology, and occasionally the type of nanoparticles [36]. These properties led to the conclusion that the optimal size for the ruthenium-based nanocarrier prepared in this work by green synthesis using HOM moss was between 70 and 80 nm. This suggests that the next experiments will be a highly effective drug for the targeted treatment of tumors. Altering the permeability of the mitochondrial membrane in the intrinsic pathway triggers apoptosis [37]. Through this mechanism, the pro- and anti-apoptotic proteins BAX and Bcl-2 decide the fate of the cell [38]. The tumor suppressor gene p53 has also been reported to trigger apoptosis by altering the expression of the BAX gene [39]. In our study, cell death was shown to follow the intrinsic mechanism leading to apoptosis. In addition, morphological signs of apoptosis were found.

In the treatment of cancer, drug resistance is a negative scenario, as resistance causes the disease to increase to uncontrollable levels. Therefore, it is crucial that effective cancer medication does not lead to drug resistance at the same time. In this study, the expression of ABCG2 was used to evaluate the drug resistance of the nanoparticles produced. Since ABCG2 inhibits the retention of multiple drugs in cells for most treatments, it leads to multidrug resistance [40]. Vascularization and membrane permeability typically develop in tumor tissues. Therefore, 10–200 nm nanoparticles tend to concentrate in tissues as passive targets [36]. As a result of the regulated release of NPs, they also have a longer half-life at the tumor site [41], and they penetrate extracellular and intracellular membranes, eliminating all processes leading to drug resistance [42]. In our study, HOM-NPs also showed a reducing effect on drug resistance.

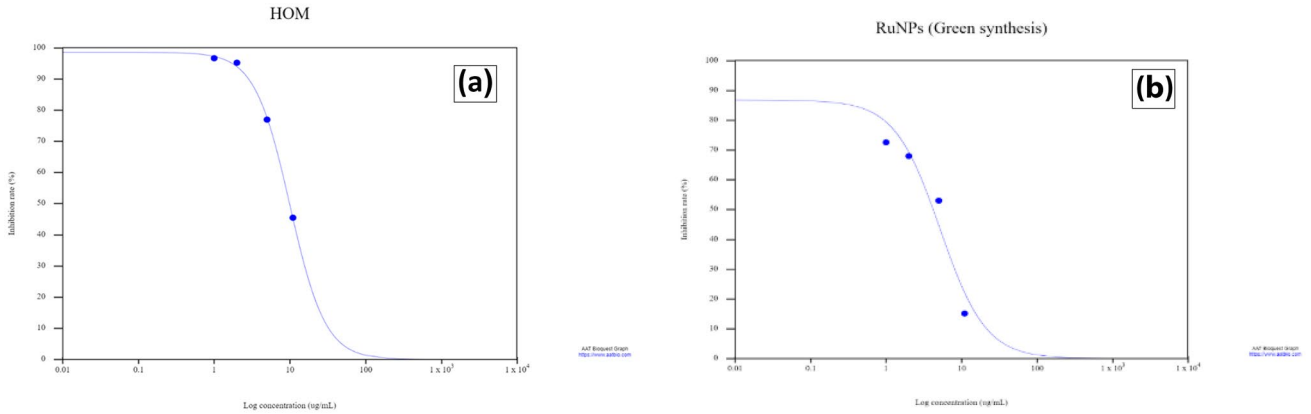

Fig. 8 IC_{50} values of HOM (**a**) and HOM-RuNPs (**b**) are shown

Conclusion

Obviously, the efficacy of chemotherapy could not be achieved due to drug resistance, and the treatment of colorectal cancer was ineffective, resulting in death in some patients. For the surviving patients, the side effects significantly affect their quality of life. In recent years, various studies have been conducted to minimize or eliminate the

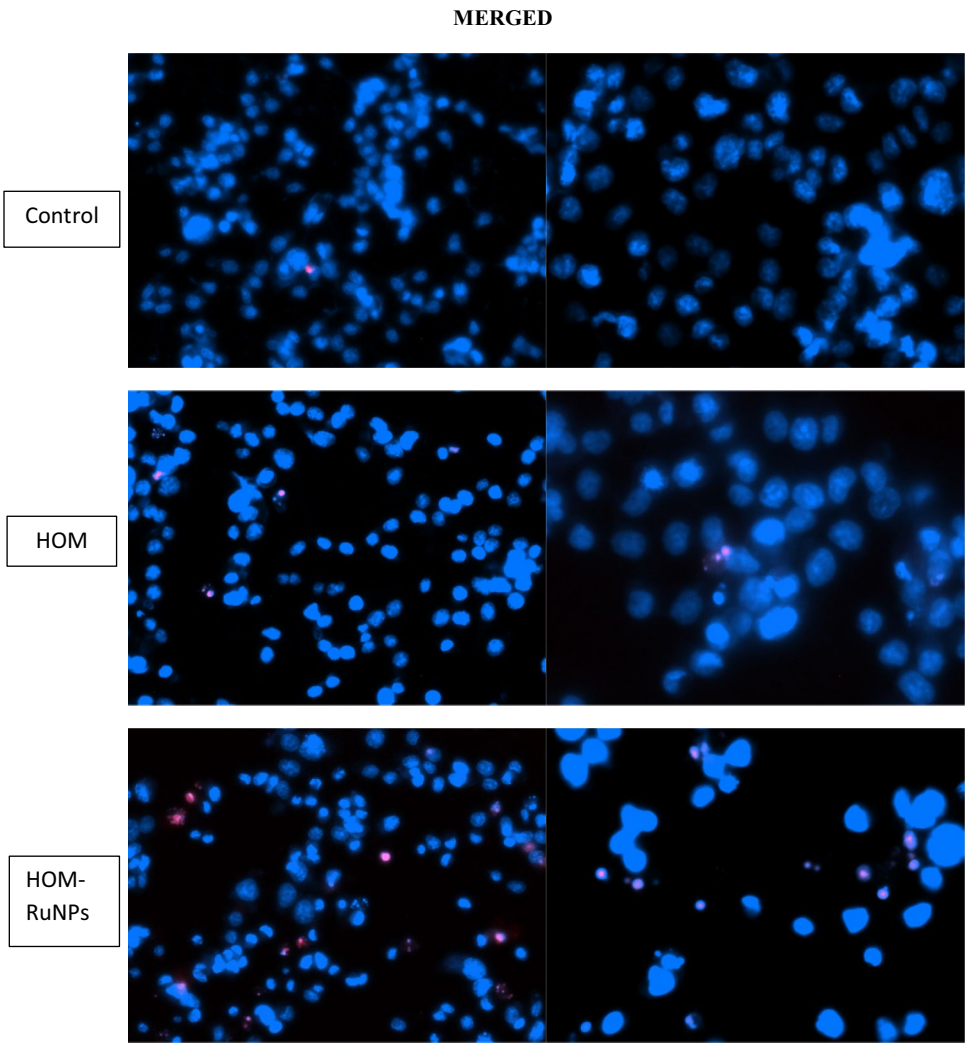

Fig. 9 Immunofluorescence images can be used to detect cell death. Late-stage apoptotic cells (secondary necrotic cells) appear pink in the double-stained images of HCT116 groups. The digits of each group have 20- and 40-fold magnification, respectively

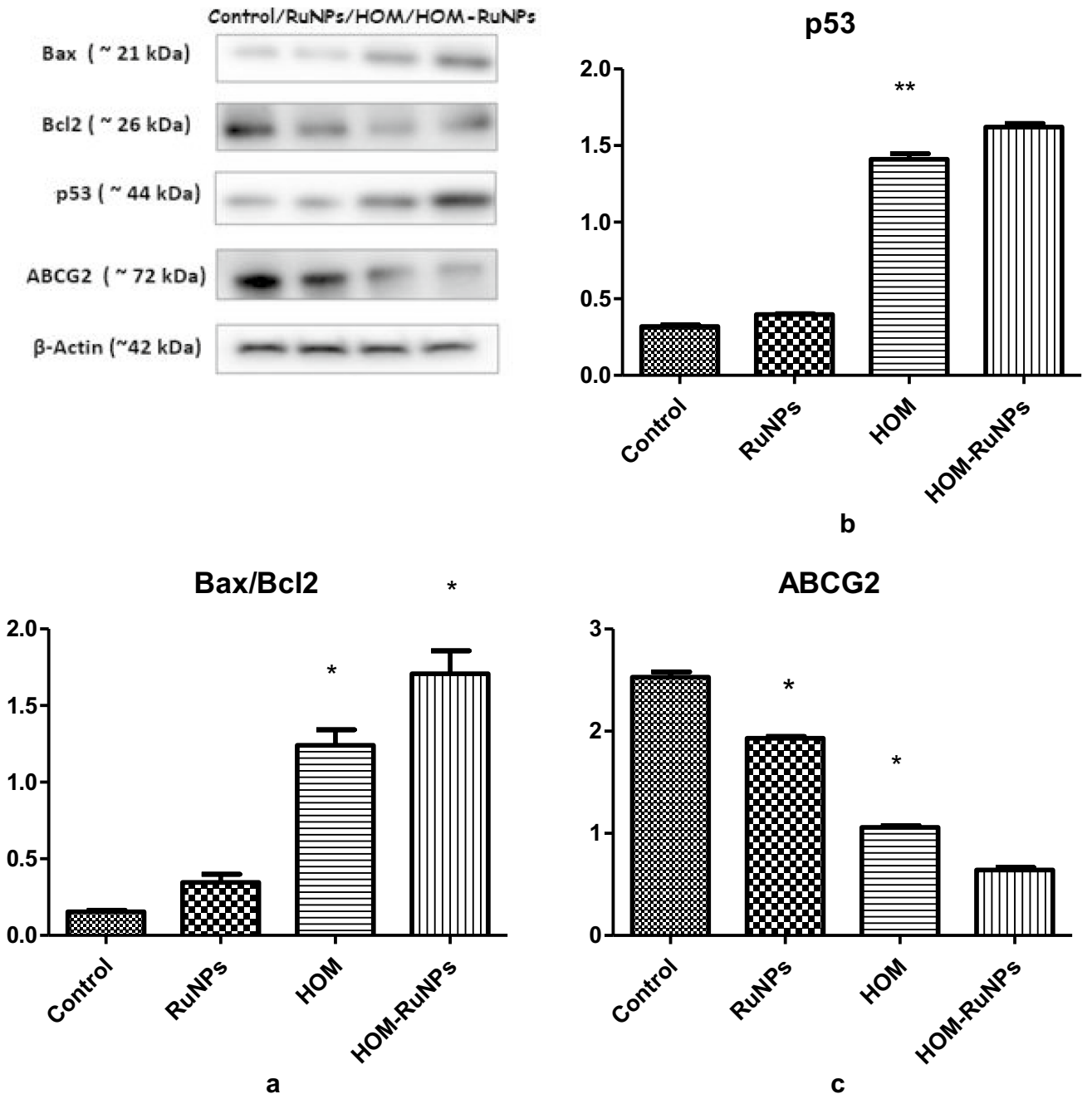

Fig. 10 It is demonstrated how HOM-RuNPs made by green synthesis affect the amounts of Bax/Bcl-2 (**a**), p53 (**b**), and ABCG2 protein expression (**c**) in HCT116 cells. (*$p < 0.005$, **$p < 0.001$, vs. control)

failure rate of chemotherapeutic agents. Nanocarriers provide very successful results with their controlled release in the target tissue. In this study, we successfully synthesized HOM-RuNPs for the first time by a green synthesis method. Considering the release profiles, cytotoxic and apoptotic effects, and drug resistance implications of HOM-RuNP nanocarriers, it may be a promising new agent for cancer therapy. In addition, we believe that the newly synthesized ruthenium nanoparticles will lead to further studies.

Funding This study is supported by the project numbered 2020/B4, Istinye University.

Data Availability All our experimental data are found in GraphPad Prism Programme.

Declarations

Conflict of Interest The authors declare no competing interests.

References

1. Siegel RL, Miller KD, Jemal A. Cancer statistics, 2017. CA Cancer J Clin Wiley. 2017;67:7–30.
2. Dekker E, Tanis PJ, Vleugels JLA, Kasi PM, Wallace MB. Colorectal cancer. Lancet [Internet]. Lancet. 2019;394:1467–80. Available from: https://pubmed.ncbi.nlm.nih.gov/31631858/.
3. Grewal S, Oosterling SJ, van Egmond M. Surgery for colorectal cancer: a trigger for liver metastases development? New ınsights into the underlying mechanisms. Biomed. 2021;9:177. Multidisciplinary Digital Publishing Institute. Available from: https://www.mdpi.com/2227-9059/9/2/177/htm.
4. Knowles G, Haigh R, McLean C, Phillips HA, Dunlop MG, Din FVN. Long term effect of surgery and radiotherapy for colorectal cancer on defecatory function and quality of life. Eur J Oncol Nurs. 2013;17:570–7. Available from: https://pubmed.ncbi.nlm.nih.gov/23453570/.
5. Malki A, Elruz RA, Gupta I, Allouch A, Vranic S, al Moustafa AE. Molecular mechanisms of colon cancer progression and metastasis: recent ınsights and advancements. Int J Mol Sci 2020;22:1–24. Available from: https://pubmed.ncbi.nlm.nih.gov/33374459/.
6. Gopal YNV, Jayaraju D, Kondapi AK. Inhibition of topoisomerase II catalytic activity by two ruthenium compounds: a ligand-dependent mode of action. Biochem. 1999;38:4382–8. Available from: https://pubmed.ncbi.nlm.nih.gov/10194357/.
7. Kostova I. Ruthenium complexes as anticancer agents. Curr Med Chem. 2006;13:1085–107. Available from: https://pubmed.ncbi.nlm.nih.gov/16611086/.
8. Santamaria R, Irace C, Montesarchio D, Paduano L, Professor A. Perspectives and potential applications of ruthenium-based nanocarriers for cancer therapy. J Pharm Drug Dev. Annex Publishers. 2013;1:1. Available from: www.annexpublishers.com.
9. Blunden BM, Stenzel MH. Incorporating ruthenium into advanced drug delivery carriers – an innovative generation of chemotherapeutics. J Chem Technol Biotechnol. John Wiley & Sons, Ltd. 2015;90:1177–95. Available from: https://onlinelibrary.wiley.com/doi/full/10.1002/jctb.4507
10. Huang S, Liang Y, Huang C, Su W, Lei X, Liu Y, et al. Systematical investigation of binding interaction between novel ruthenium(II) arene complex with curcumin analogs and ctDNA. Luminescence. John Wiley & Sons, Ltd. 2016;31:1384–94. Available from: https://doi.org/10.1002/bio.3119.
11. Xu Z, Huang J, Kong D, Yang Y, Guo L, Jia X, et al. Potent half-sandwich Ru(II) N^N (aryl-BIAN) complexes: lysosome-mediated apoptosis, in vitro and in vivo anticancer activities. Eur J Med Chem. 2020;207. Available from: https://pubmed.ncbi.nlm.nih.gov/32882612/.
12. Tarasenko NV, Butsen AV, Nevar EA, Savastenko NA. Synthesis of nanosized particles during laser ablation of gold in water. Appl Surf Sci. North-Holland. 2006;252:4439–44.
13. Korbekandi H, Iravani S, Abbasi S. Production of nanoparticles using organisms. [Internet]. Taylor & Francis. 2009;29:279–306. Available from: https://doi.org/10.3109/07388550903062462.
14. Razavi M, Salahinejad E, Fahmy M, Yazdimamaghani M, Vashaee D, Tayebi L. Green chemical and biological synthesis of nanoparticles and their biomedical applications. Green Processes for Nanotechnology: From Inorganic to Bioinspired Nanomaterials [Internet]. Springer International Publishing. 2015;207–35. Available from: https://doi.org/10.1007/978-3-319-15461-9_7.
15. Hussain I, Singh NB, Singh A, Singh H, Singh SC. Green synthesis of nanoparticles and its potential application. Biotechnol Lett [Internet]. Springer Netherlands. 2016;38:545–60. Available from: https://doi.org/10.1007/s10529-015-2026-7.
16. Narayanan KB, Sakthivel N. Green synthesis of biogenic metal nanoparticles by terrestrial and aquatic phototrophic and heterotrophic eukaryotes and biocompatible agents. Adv Colloid Interface Sci Elsevier. 2011;169:59–79.
17. Mittal AK, Chisti Y, Banerjee UC. Synthesis of metallic nanoparticles using plant extracts. Biotechnol Adv Elsevier. 2013;31:346–56.
18. Singh SO. Invitation for book chapter on bryophytes view project. Article in Int J Pharm Sci Rev Res. 2013;23:28–35. Available from: www.globalresearchonline.net.
19. Özerkan D, Erol A, Altuner EM, Canlı K, Kuruca DS. Some bryophytes trigger cytotoxicity of stem cell-like population in 5-fluorouracil resistant colon cancer cells. Taylor & Francis. 2021;74:1012–22. Available from: https://doi.org/10.1080/01635581.2021.1933098.
20. Oztopcu-Vatan P, Savaroglu F, Filik-Iscen C, Kabadere S, Ilhan S, Uyar R. Antimicrobial and Antiproliferative Activities of Homalothecium Sericeum (Hedw.) Schimp. EXTRACTS.
21. Gür M, Verep D, Güney K, Güder A, Murat Altuner E. Determination of some flavonoids and antimicrobial behaviour of some plants' extracts. Indian J Pharm Educ Res. 2023;51. Available from: www.ijper.org.
22. Orellana EA, Kasinski AL. Sulforhodamine B (SRB) Assay in cell culture to ınvestigate cell proliferation. Bio Protoc [Internet]. NIH Public Access; 2016 [cited 2022 Dec 12];6. Available from: https://pmc/articles/PMC5448418/.
23. Joshi PS, Sutrave DS. A comparative study of structural and morphological properties of pristine and Mn doped ruthenium oxide thin films. Int J Thin Fil Sci Tec. 2017;6(2):83–6.
24. Chen B, Le W, Wang Y, Li Z, Wang D, Ren L, et al. Targeting negative surface charges of cancer cells by multifunctional nanoprobes. Theranostics. 2016;6:1887–98. Available from: https://pubmed.ncbi.nlm.nih.gov/27570558/.
25. Crowley LC, Marfell BJ, Waterhouse NJ. Analyzing cell death by nuclear staining with Hoechst 33342. Cold Spring Harb Protoc. 2016;2016. Available from: http://cshprotocols.cshlp.org/content/2016/9/pdb.prot087205.full.
26. Gour A, Jain NK. Advances in green synthesis of nanoparticles. [Internet]. Taylor & Francis. 2019;47:844–51. Available from: https://doi.org/10.1080/21691401.2019.1577878.
27. Singh A, Jain D, Upadhyay MK, Khandelwal N, Verma HN. Green synthesis of silver nanoparticles using argemone mexicana leaf extract and evaluation of their antimicrobial activities. Dig J Nanomater Biostruct. 5:483–9.
28. Schott O, Ferrando-Soria J, Bentama A, Stiriba SE, Pasán J, Ruiz-Pérez C, et al. Chromium(III) complexes with 2-(2′-pyridyl) imidazole: synthesis, crystal structure and magnetic properties. Inorganica Chim Acta Elsevier. 2011;376:358–66.
29. Thangavel P, Viswanath B, Kim S. Recent developments in the nanostructured materials functionalized with ruthenium complexes for targeted drug delivery to tumors. Int J Nanomedicine. Dove Press. 2017;12:2749. Available from: https://pmc/articles/PMC5388259/.
30. Aird RE, Cummings J, Ritchie AA, Muir M, Jodrell DI, Morris RE, et al. In vitro and in vivo activity and cross resistance profiles of novel ruthenium (II) organometallic arene complexes in human ovarian cancer. Br J Cance. Nature Publishing Group. 2002;86:1652. Available from: https://pmc/articles/PMC2746580/.
31. Ali MYS, Anuradha V, Abishek R, Yogananth N, Sheeba H. In vitro anticancer activity of green synthesis ruthenium nanoparticle from Dictyota dichotoma marine algae. NanoWorld J. United Scientific Group. 2017;03.
32. Kannan SK, Sundrarajan M. Green synthesis of ruthenium oxide nanoparticles: characterization and its antibacterial activity. Advanced Powder Technology Elsevier. 2015;26:1505–11.
33. Gopinath K, Karthika V, Gowri S, Senthilkumar V, Kumaresan S, Arumugam A. Antibacterial activity of ruthenium nanoparticles synthesized using Gloriosa superba L. leaf extract. J Nanostructure Chem. Springer Medizin. 2014;4:1–6. Available from: https://doi.org/10.1007/s40097-014-0083-4.

34. Karges J, Díaz-García D, Prashar S, Gómez-Ruiz S, Gasser G. Ru(II) Polypyridine complex-functionalized mesoporous silica nanoparticles as photosensitizers for cancer targeted photodynamic therapy. ACS Appl Bio Mater Am Chem Soc. 2021;4:4394–405. Available from: https://doi.org/10.1021/acsabm.1c00151.
35. Wu J. The enhanced permeability and retention (EPR) effect: the significance of the concept and methods to enhance ıts application. J Pers Med. 2021;11:771. Multidisciplinary Digital Publishing Institute. Available from: https://www.mdpi.com/2075-4426/11/8/771/htm.
36. Subhan MA, Yalamarty SSK, Filipczak N, Parveen F, Torchilin VP. Recent advances in tumor targeting via EPR effect for cancer treatment. J Pers Med. 2021;11:571. Multidisciplinary Digital Publishing Institute. Available from: https://www.mdpi.com/2075-4426/11/6/571/htm.
37. Dadsena S, King LE, García-Sáez AJ. Apoptosis regulation at the mitochondria membrane level. Biochimica et Biophysica Acta (BBA) - Biomembranes. Elsevier. 2021;1863:183716.
38. Askari N, Shafieipour S, Aghajanpour M. Role of BAX, BCL-2, and MICAL-2 genes in esophageal cancer. Res Med. 2019;43:170–6. Available from: http://pejouhesh.sbmu.ac.ir/article-1-1954-en.html.
39. Yang T-T, Namba H, Hara T, Takmura N, Nagayama Y, Fukata S, et al. p53 induced by ionizing radiation mediates DNA end-jointing activity, but not apoptosis of thryroid cells. 1997.
40. Taylor NMI, Manolaridis I, Jackson SM, Kowal J, Stahlberg H, Locher KP. Structure of the human multidrug transporter ABCG2. Nature. Nature Publishing Group. 2017;546:504–9. Available from: https://europepmc.org/article/med/28554189.
41. Akbarzadeh A, Rezaei-Sadabady R, Davaran S, Joo SW, Zarghami N, Hanifehpour Y, et al. Liposome: classification, preparation, and applications. Nanoscale Res Lett. Springer New York LLC. 2013;8:1–9. Available from: https://doi.org/10.1186/1556-276X-8-102.
42. Kesharwani SS, Kaur S, Tummala H, Sangamwar AT. Overcoming multiple drug resistance in cancer using polymeric micelles. Taylor & Francis. 2018;15:1127–42. Available from: https://doi.org/10.1080/17425247.2018.1537261.